Seismic Real-Time Monitoring of the Habanero#4 Stimulation - Technical Report

Q-con GmbH

Geothermal reservoir engineering

GDY034

Report title:	Seismic Real-Time Monitoring of the Habanero#4 Stimulation - Technical Report
Author(s):	Stefan Baisch, Henrik Stang
Report date:	14th June 2013
Project:	Habanero#4
Prepared for:	Geodynamics Ltd.
Version:	1
Archive No.:	GDY034

Contents

1 SUMMARY

Between November 13th, 2012 and November 30th, 2012, the Habanero#4 well was hydraulically stimulated. Induced seismicity was monitored in real-time with a local 7 station network transmitting continuous waveform data to a central acquisition office located in the Habanero camp. Additional, 17 offline stations were operated at larger distances in order to constrain the fault mechanisms of the induced seismicity.

The current report documents the technical operation of the live monitoring stations and the real-time processing of the data. Processing of data recorded by offline stations and more detailed data analyses have been performed after the operation was terminated and are provided in a separate report (GDY035).

The live monitoring system was operated in 24/7 mode by two seismologists in the field supported by two seismologists working from the Q-con offices in Germany. Remote access from the German office was established by satellite link. Data was processed with Q-con's in-house software package QUBE. Despite the extremely high seismic event rate of more than 2,700 events/day during peak-times, data processing was performed in real-time and the processing results (i.e. seismic event detections, hypocenter locations, event magnitudes) were provided to Geodynamics Ltd. on a daily basis as part of short-reports, which are attached to this document (Section 6). All automatically determined phase onset times were quality controlled by visual inspection and manually adjusted whenever necessary.

Additionally, the QUBE traffic light system was operated to stop hydraulic operations in case the magnitude of the induced seismicity reached the pre-defined critical level of M_L=3.7. The occurrence of events with magnitudes exceeding M_L≥2.5 (yellow traffic light) was reported to Geodynamics Ltd. within less than four minutes. On November 27th, 2012 8:03 UTC, the traffic light status switched to yellow due to the occurrence of a magnitude M_L=3.0 event.

The monitoring system was operated without noteworthy technical issues and the system had no downtimes during the monitoring period. Event triggering was performed using an STA/LTA based detector without triggering dead-time. A total number of 27,445 reservoir events were detected with magnitudes ranging from M_L=-1.6 to M_L=3.0. The signal-to-noise ratio of 20,734 of these events was sufficient for determining hypocenter locations. The resulting seismicity forms a subhorizontal cloud around the injection well with a lateral extension of approx. 2 square-kilometres. The (apparent) vertical extension is in the order of several hundreds of metres and is dominated by the hypocenter location accuracy. Seismic activity is highly organized in space and time, starting close to the injection well and subsequently migrating away. These characteristics are consistent with previous observations made during hydraulic stimulations in the same reservoir.

2 SEISMIC STATION NETWORK

Seismic monitoring of geothermal activities in the Cooper Basin started already in the year 2003. The initial monitoring system installed and operated by Tohoku University (Japan) was operated only for a short-period of time during the first stimulation of the Habanero#1 well (compare Baisch et al., 2006). In April 2005 the monitoring system was significantly upgraded and all stations have been recording time-continuous data since then.

With the beginning of operational activities in neighbouring wells, additional seismic monitoring stations were installed in the years 2008 and 2009, extending the existing station network towards the West. Only recently, 8 additional mobile stations were temporarily deployed for monitoring the Habanero#4 stimulation. The locations of these stations were chosen in order to improve the coverage of the focal sphere when determining fault plane solutions. Additionally, 3 of these stations were placed approx. 15 km to the NW of Habanero#4 in a region, where seismicity has occurred previously.

Due to the stepwise extension of the station network, several generations of hardware are currently being used. While the surface design and configuration of all stations is similar (see next section), different type of recording sensors are used. Most seismic stations are operated with downhole geophones, which are deployed in shallow wells (depth range in the order of 90 m to 370 m). The mobile stations installed recently are equipped with surface seismometers. Figure 1 shows the location of the seismic monitoring stations.
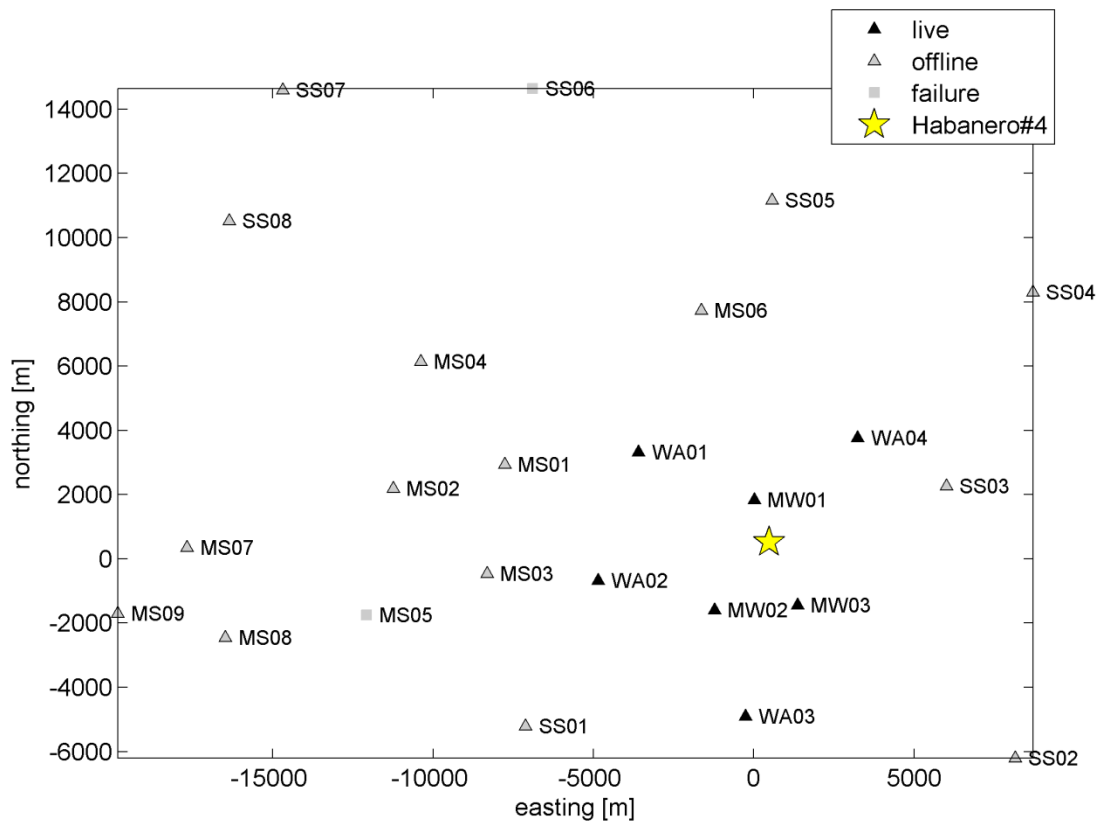
Figure 1: Map of seismic station locations. Live stations are denoted by black triangles, offline stations by grey triangles. Stations MS05 and SS06 were not operated due to hardware failure. Coordinates are given relative to the Habanero#1 wellhead. Stations SS01-SS08, MS06 and WA03 are operated with surface seismometers, all other stations are equipped with downhole geophones.

2.1 Monitoring Stations

The seismic stations are designed as zero-maintenance stand-alone units for continuous operation. The general design is shown in Figure 2. Stations are powered by solar panels in combination with back-up batteries. All stations are equipped with 3 channel SMART24-R® data recorders (Geotech Instruments) where continuous data recordings are GPS time-stamped and locally stored on a removable hard-disk. In parallel, live stations can transmit real-time data by WLAN to the central acquisition office located at the Habanero camp site.

All stations are operated with a sampling rate of 500 Hz resulting in a storage capacity of the removable hard disks of 2-4 months. In offline recording mode, data is directly downloaded at the station locations. The data recording format is cd1.1 with a file length of 5 minutes. Besides the waveform data, the data acquisition also creates low-level logfiles including state-of-health information.

The stations are equipped with different types of sensors. These include downhole geophones as well as surface seismometers. Details of each sensor are given in the station specification sheets in section 5.
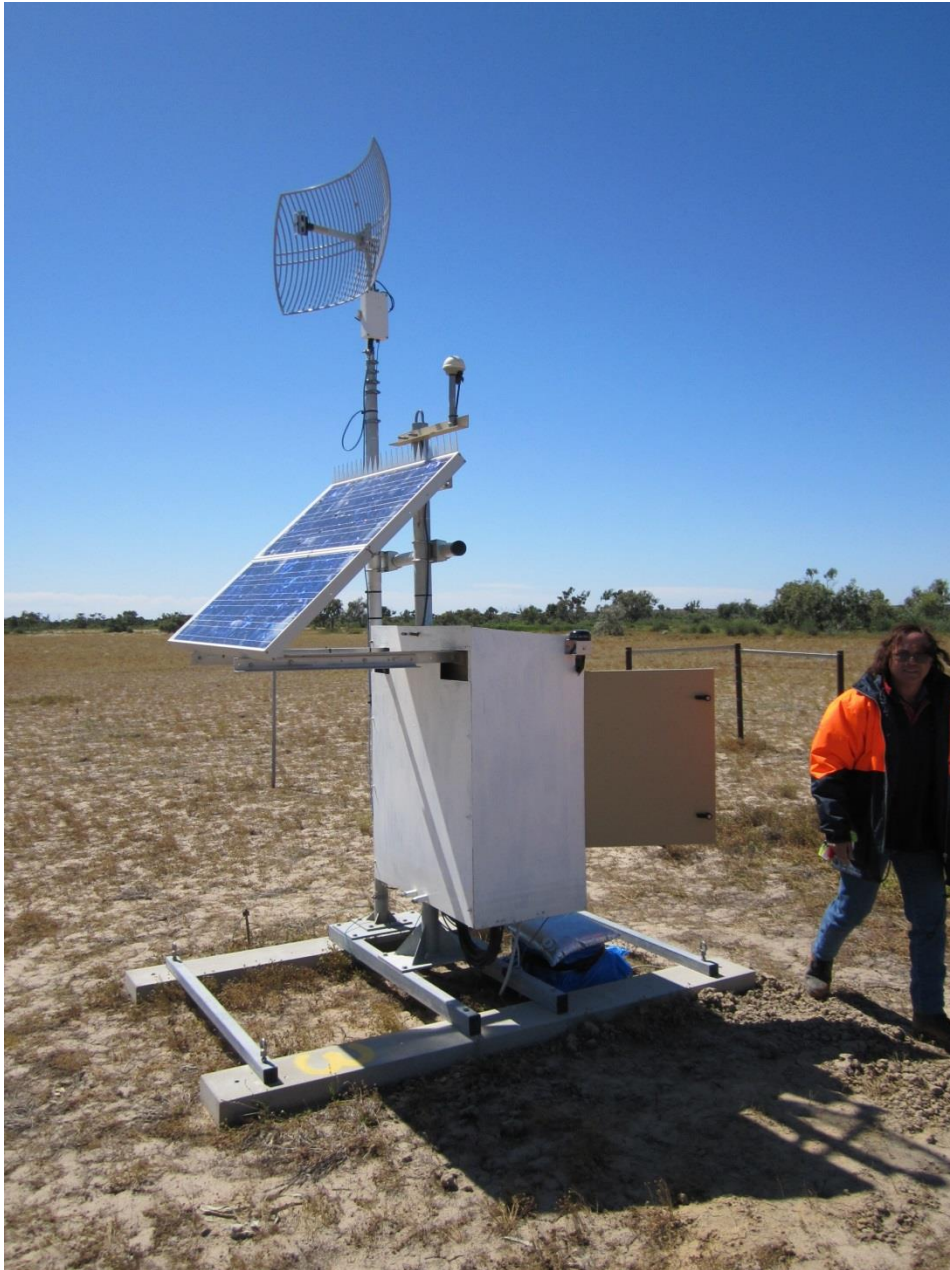
Figure 2: Example of the seismic station design. The surface assembly is mounted on concrete sleeves with all electronics mounted inside the cabinet. Stations are powered by solar panels in combination with back-up batteries. Continuous data recordings are GPS time-stamped and stored locally on a removable hard-disk. In parallel, real-time data is transmitted by WLAN to the central acquisition office located at the Habanero camp site.

2.2 Central Acquisition Office

Figure 3 shows the general set up of the seismic monitoring system. Real-time data was transmitted by WLAN from the seismic stations to the central acquisition computer located in the monitoring container at the Habanero camp site.

The continuous raw data was transmitted in cd1.1 file format with 10 s data frame length. A low-level acquisition software provided by Geotech Instruments LLC was storing raw data into a *mysql* data base. Waveform sections of all stations were automatically exported into SEGY data files every 3 minutes, which were passed to the QUBE data base for further processing. The SEGY files provided the data for real-time processing.

Data processing was performed by Q-con's software package QUBE. The master QUBE automatically

- run the event detector (for details see section 3.2.1),
- determined P- and S-phase onset times (for details see section 3.2.2),
- determined the hypocenter location (for details see section 3.2.3),
- determined the event magnitude (for details see section 3.2.4),
- and operated the traffic light system (for details see section 3.2.5).

In addition to the master QUBE, four slave QUBEs were set up for simultaneously working on the database (see section 3.2). Two of the slave QUBEs were set up in the Q-con office in Germany connected by satellite link.

Communication between the Habanero seismic office and the stimulation manager's office was established by radio and (portable) telephone. The communication between the German Q-con office and the stimulation manager's office was established by (portable) telephone and email.

Several measures were in place for mitigating the risk of technical failures. These include:

- A back-up copy of all seismic raw data was stored at the seismic station locations.
- The QUBE event data base was automatically mirrored in real-time to an independent server located in the German office.
- Local back-up copies of the QUBE database were created on a daily basis.
- All computers and network devices were protected by UPS from failure of the diesel generators providing power to the camp. With the capacity of the UPS, the entire monitoring system could be powered for approx. 15 minutes.
- Spare parts for all critical elements of the seismic monitoring system (incl. acquisition & processing computers, central WLAN antenna, etc.) were pre-configured and stored on location.
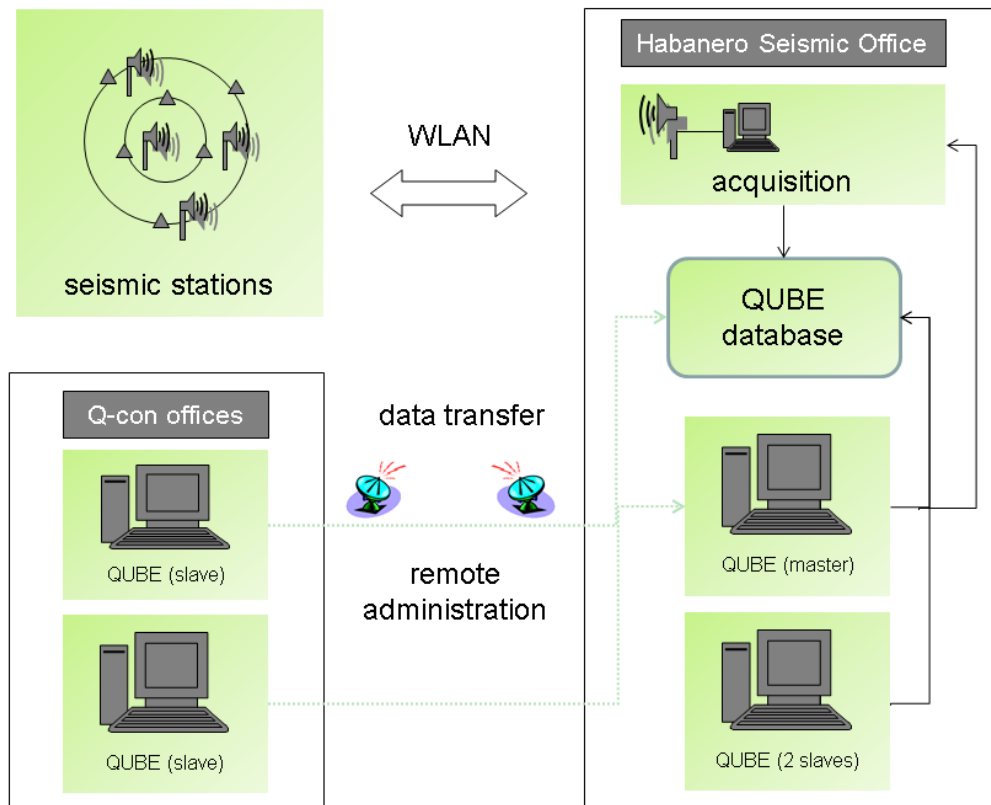
Figure 3: Sketch of the setup of the seismic monitoring system. The data base and the master QUBE PC were located in the Habanero field office. Real-time data was streamed from the monitoring stations to the acquisition computer by WLAN. Four slave QUBEs were set up for simultaneously working on the database. Two of the slave QUBEs were set up in the Q-con office in Germany connected by satellite link.

2.3 Seismic Raw Data Format

Seismic raw data was stored in cd1.1 format on the local hard disks at each station location (see Table 1) and waveform sections of the live data stream were stored in SEGY format on the acquisition computer (see Table 2).

Since the SEGY data files were written in real-time, a delayed data package from a station, e.g. due to a transmission issue, could cause a data gap in the SEGY files. Small data gaps typically occurred during the daily clean-up process of the *mysql* data base. These data gaps always occurred for only a single station at a time.

If a seismic event occurred in a time window where the waveform section is incomplete, then the data from the missing station was back-filled as part of the automatic processing with QUBE. For this, missing data was retrieved by ftp from the associated station and written into the QUBE event file data base.

cd1.1 data format	
name convention	YYYYMMDD_hhmmss_C_[station code].cd11
number of channels	3
channel order	v, h1, h2
unit	counts
file size	5 minutes = 150,000 samples

Table 1: Description of the cd1.1 raw data format. Data files of this format were stored at the station locations.

SEGY data format	
name convention	YYYYMMDD_hhmmss _JOLO01.segy
number of channels	24
channel order	1 MW1 – v
	2 MW1 – h1
	3 MW1 – h2
	4 MW2 – v
	5 MW2 – h1
	6 MW2 – h2
	7 MW3 – v
	8 MW3 – h1
	9 MW3 – h2
	10 WA3 – v
	11 WA3 – h1
	12 WA3 – h2
	13 WA4 – h1
	14 WA4 – v
	15 WA4 – h2
	16 S06 – v empty
	17 S06 – h1 empty
	18 S06 – h2 empty
	19 WA1 – v
	20 WA1 – h1
	21 WA1 – h2
	22 WA2 – v
	23 WA2 – h1
	24 WA2 – h2
unit	counts
file size	5 minutes = 150,000 samples

Table 2: Description of the SEGY data format. Data files of this format were stored on the acquisition computer.

3 SEISMIC MONITORING

Between November 13th, 2012 and November 30th, 2012, the Habanero#4 well was hydraulically stimulated. During this period of time, real-time monitoring was performed. The live monitoring system was operated in 24/7 mode by 2 seismologists in the field supported by 2 seismologists working from the Q-con office in Germany. Remote access from the German offices was provided by satellite link (compare Figure 3).

Due to the high seismic activity rate at the end of the stimulation, the real-time monitoring system was operated in a fully automatized mode for another 4 days. The current report documents the monitoring period from November 12th, 2012 (13:30 UTC) until December 4th, 2012 (7:30 UTC).

3.1 System State of Health

The system state of health (SOH) was continuously monitored during the real-time operation. This included the following parameters:

- battery voltage at the monitoring stations,
- GPS signal reception at the monitoring stations and the time drift of the internal clock module of the data loggers,
- temperature inside the monitoring stations,
- WLAN data transmission.

Figure 4 shows the SOH parameters of the live stations during the monitoring period. The monitoring system was operated without significant technical issues and the station network had no downtimes during the monitoring period (compare Figure 5, Table 3 and Table 4).

The following technical issues occurred during the monitoring period:

- The data logger at station WA01 had an internal disk writing error at the beginning of the stimulation causing missing offline data (cd1.1 format). The associated data, however, was transmitted in real-time to the acquisition office and exists in the data base in SEGY format. The writing error was fixed on November 13th, 2012.

- Station MW01 showed occasional WLAN data transmission problems resulting in a temporal loss of real-time data for a short period of time. The associated data, however, exists in cd1.1 format. The station had to be rebooted several times in the course of fixing the transmission problem.

- On November 19th, 2012 (19:50 UTC) the main radio for WLAN data transmission dropped out. WLAN data transmission was re-established after 3 minutes and all data was backfilled into the QUBE database. Effectively, this issue resulted in a 3

minute delay of the data processing (for the time window November 19th, 19:50 UTC to 19:55 UTC) but caused no system downtime.

- Several short power failures occurred during the monitoring period, all of which had no impact on the seismic monitoring system due to the installed UPS protection.

Already prior to the monitoring period, it was recognized that channel h1 of station MW01 exhibits reduced sensitivity most likely associated with a damaged cable. Similarly, channel h1 of station WA03 showed reduced sensitivity which may be related to a tilt of the seismometer vault caused by subsidence after a major flooding event. Both issues could not be fixed prior to the monitoring period. Therefore, channel h1 of station MW01 and all channels of station WA03 were not used for the analysis of dynamic seismic event properties (i.e. magnitude, seismic moment). These channels were only used for kinematic data analysis (i.e. phase onset identification). The seismometer at station WA03 was re-placed on December 3rd, 2012.
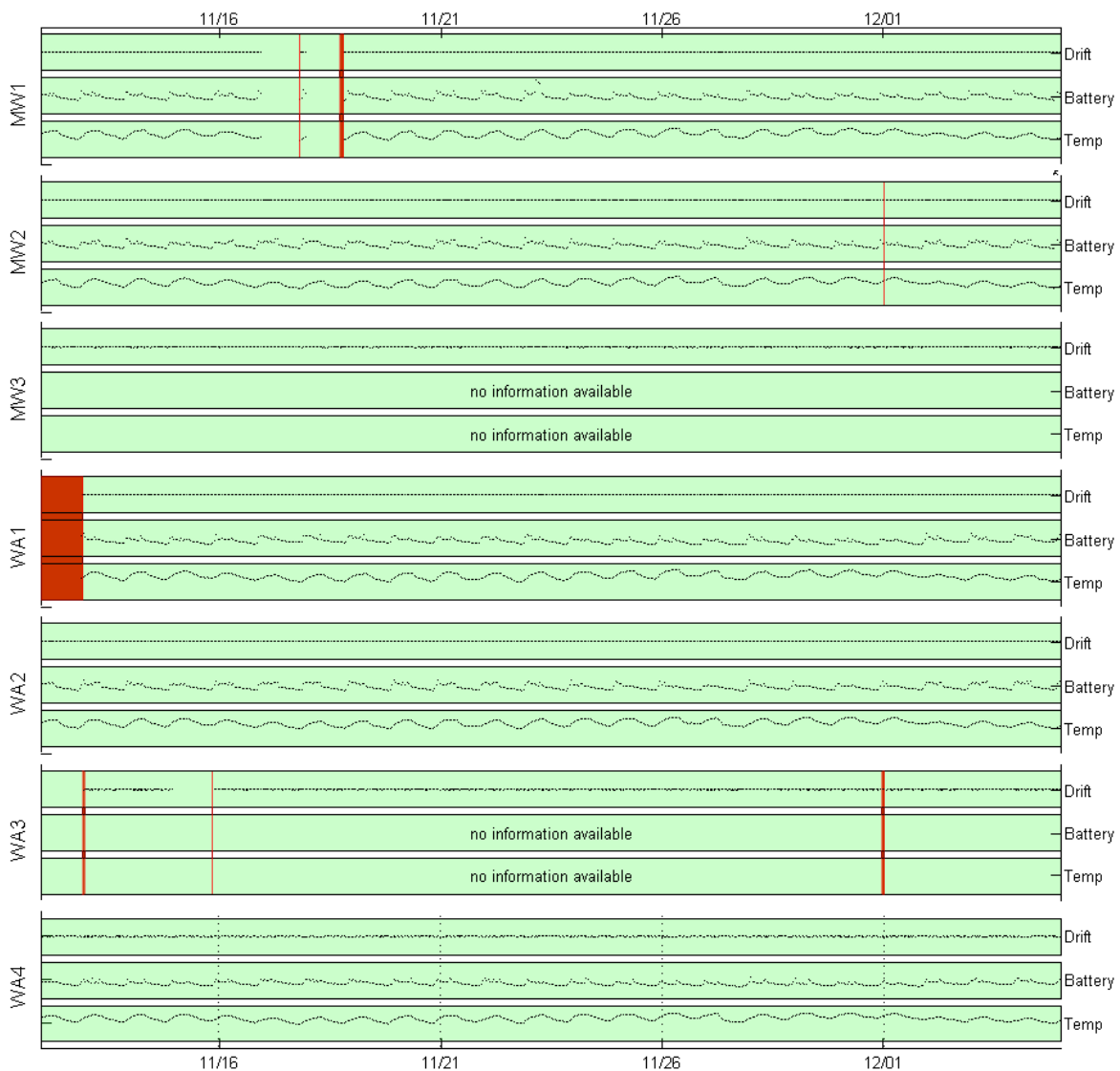
Figure 4: cd1.1 data availability and state of health (SOH) of the live stations as a function of time between November 12th, 2012 and December 4th, 2012. The diagrams (black dots) show upper and lower threshold bounds for the internal time drift (top; +/- 0.1 millisecond), battery voltage (middle; 10/16 V) and temperature (bottom; 0°C/65°C). Green shading denotes normal functionality. Red shading indicates missing cd1.1 data. Note that the large data gap at station WA1 is related to a disk writing error of the data logger. For the associated period of time, data was transmitted in real-time to the acquisition office and exists in the data base in SEGY format. Due to a different firmware version, battery voltage and temperature readings were not logged by stations MW03 and WA03, respectively. During real-time monitoring, these SOH parameters were regularly checked by remotely accessing the data loggers.
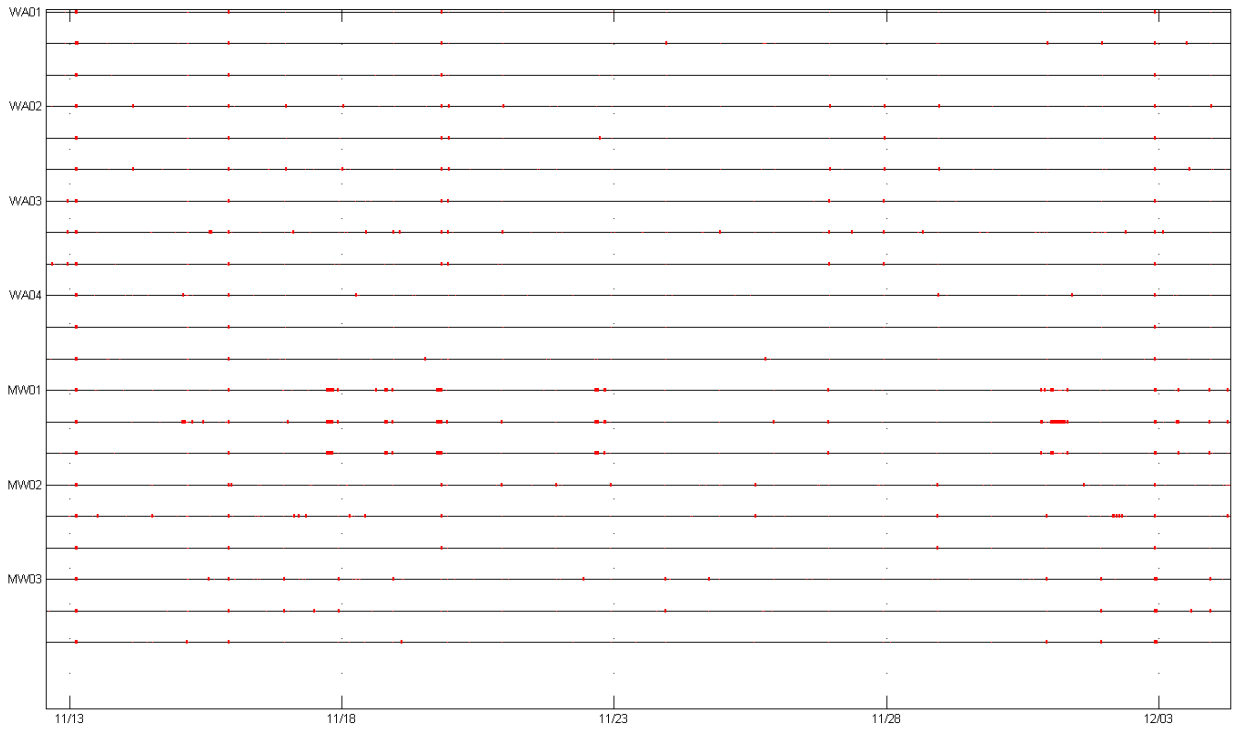
Figure 5: Real-time data (SEGY format) availability of the live stations as a function of time between November 12th, 2012 (13:30 UTC) and December 4th, 2012 (07:30 UTC). Data gaps are marked in red.

station	real-time data availability
WA01	99.41
WA02	99.21
WA03	99.00
WA04	99.34
MW01	99.75
MW02	99.13
MW03	99.14

Table 3: Real-time data availability (SEGY format) of the live stations.

station	offline data availability
MW01	99.55
MW02	99.90
MW03	100.00
WA01	98.32
WA02	100.00
WA03	99.70
WA04	100.00

Table 4: Offline data availability (cd1.1 format) of the Habanero seismic stations in the time interval between November 12th, 2012 and December 4th, 2012.

3.2 Data Processing

Data was processed with Q-con's in-house software package QUBE. The QUBE software consists of different modules for automatized and user-interactive data processing, respectively. Figure 6 summarizes the data processing steps. Despite the extremely high seismic event rate of more than 2,700 events/day during peak-times, all data processing was performed in real-time and the processing results (i.e. seismic event detections, hypocenter locations, event magnitudes) were provided to Geodynamics Ltd. on a daily basis (compare section 6). Details of the processing steps are described in the following sections.
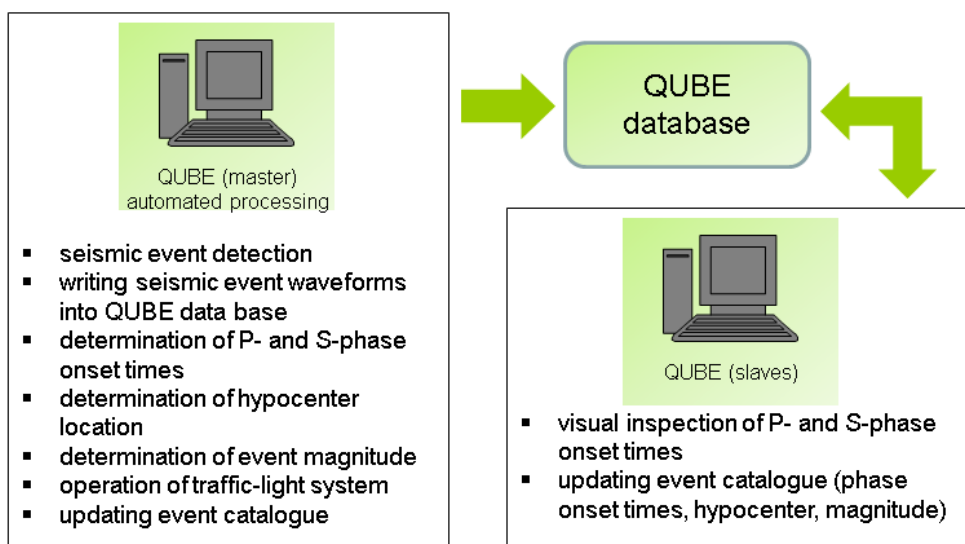
Figure 6: Schematic diagram summarizing data processing.

3.2.1 Event Detector

The event detector was based on an STA/LTA algorithm. A seismic event was declared whenever coincident STA/LTA detections on at least 3 trigger channels occurred. The trigger channels used during real-time monitoring are summarized in Table 5. Figure 7 shows the master QUBE, displaying waveforms during real-time monitoring. Within the shown time window of 3 minutes length, 7 seismic events were detected. The detector was operated without invoking a "deadtime" and the minimum time difference between 2 subsequent detections was 1 second, while the event seismogram length was 9 seconds. This configuration allowed reliable event detection even when the seismicity rate was extremely high and waveforms of different seismic events were overlapping (see example waveforms in Figure 8 and Figure 9).

station	trigger channel
WA01	v, h1
WA02	v, h1
WA03	-
WA04	v
MW01	v, h1
MW02	v
MW03	v, h1

Table 5: Trigger channels used during real-time monitoring.
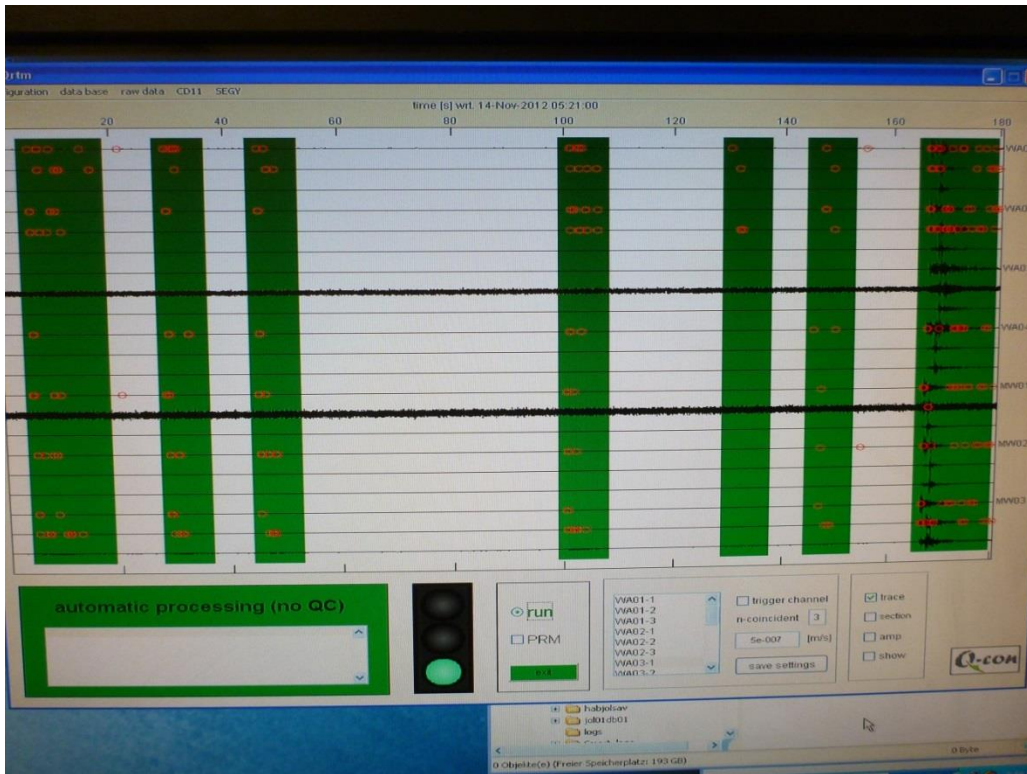
Figure 7: Photograph showing the waveform display of the master QUBE. On each trigger channel, STA/LTA detections are indicated by red circles. Green shading denotes those time windows for which a seismic event is declared due to coincident STA/LTA detections. The master QUBE also shows the traffic light status. Note the high event rate of seven reservoir events occurring in this 3 minutes time window.

3.2.2 Picking Phase Arrival Times

After event detection, P- and S-phase onset times were automatically determined with the QUBE autopicker. The underlying algorithms are based on different signal-processing methods in combination with a pattern recognition technique, which can be trained by the analyst. Since the QUBE software is not publicly available, we do not provide further details. We note, however, that a detailed understanding of the autopicker is not required here since all automatically determined phase onset times were quality controlled by visual inspection and manually adjusted whenever necessary (compare Figure 6).

The picking accuracy is critically depending on event magnitudes. For seismograms with low signal-to-noise ratio, the accuracy decreases because phase onsets might be masked by seismic background noise. Also for the largest magnitude events, the picking accuracy slightly decreases due to the dominating low-frequency signal contributions and a more complicated source function. On average, we estimate that the picking accuracy is in the order of 8 ms for P- and 16 ms for S-phase onsets, respectively. Additionally, errors may arise from false association of phase onsets. This may occur especially during times of

high seismicity rate when the waveforms of different events are overlapping (compare waveform examples shown in Figure 8 and Figure 9). However, we estimate that the rate of false phase association is << 1%.
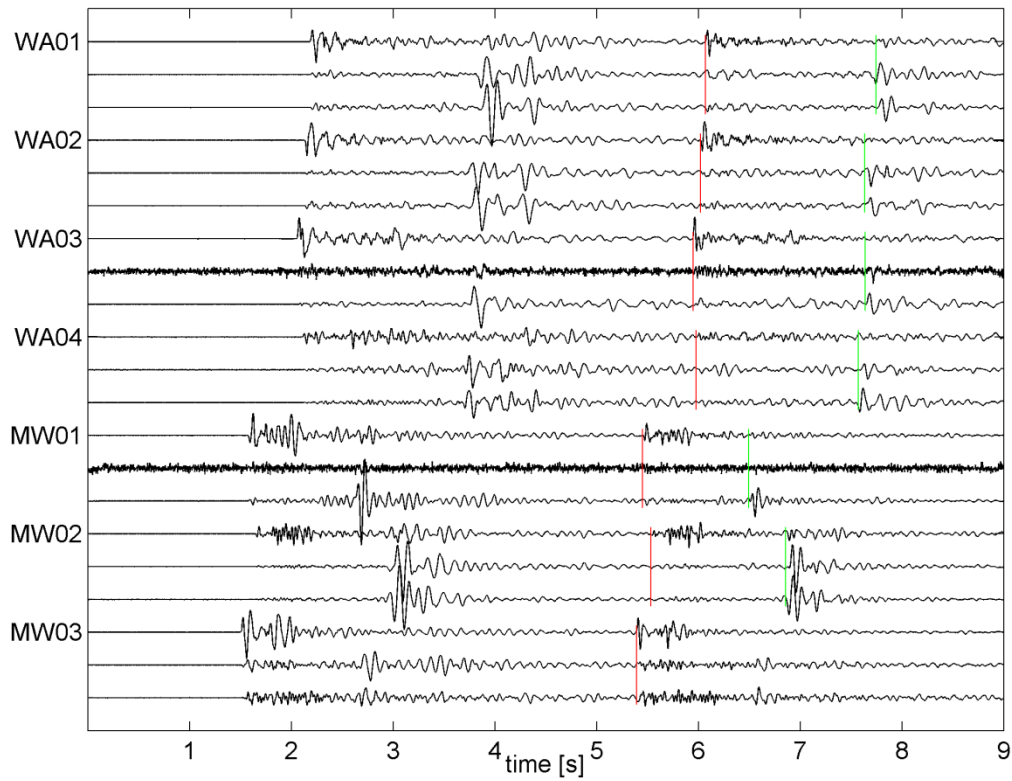
Figure 8: Example of a trace-normalized waveform section of an M_L=0.9 reservoir event followed by a second event with M_L=0.6. P- and S-phase onset times of the second event are indicated by red and green lines, respectively. Absolute hypocenter locations of the two events differ by approx. 20 m.
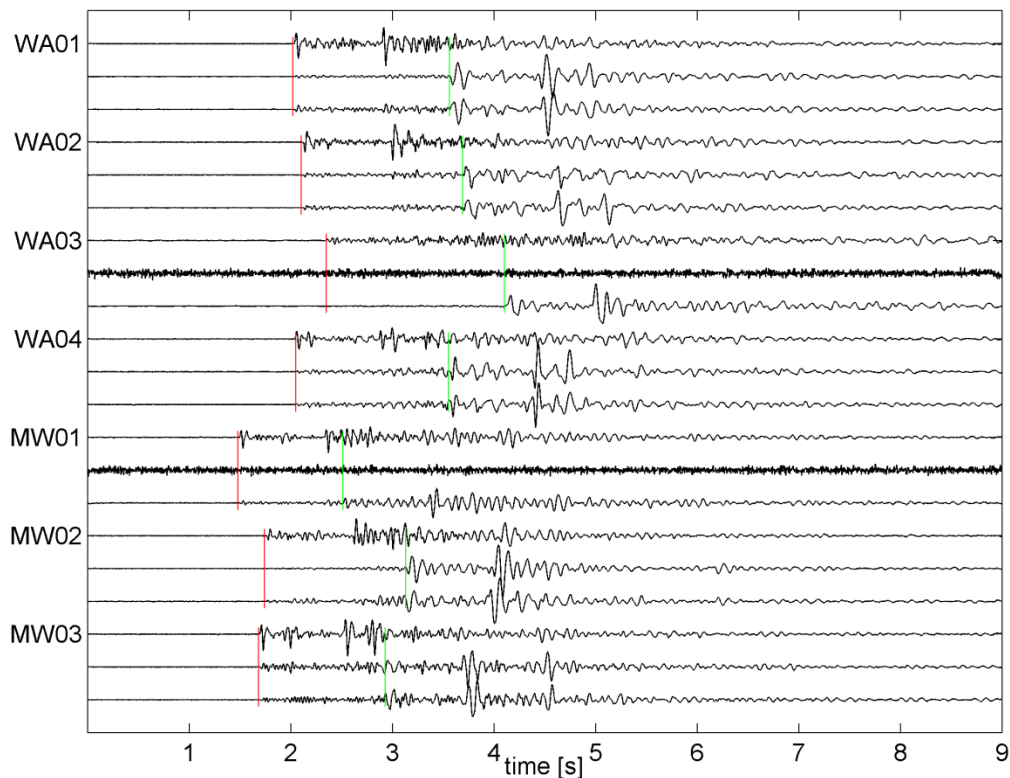
Figure 9: Example of a trace-normalized waveform section of an M_L=0.3 reservoir event followed by a second event with M_L=0.4. P- and S-phase onset times of the first event are indicated by red and green lines, respectively. P- and S-phase onsets of the second event are partially masked by the coda of the first event. Absolute hypocenter locations of the two events differ by approx. 200 m. However, identifying phase onsets of the second event is complicated due to an interference with the coda of the first event thus adding a potential bias to the hypocenter location.

3.2.3 Determination of Hypocenter Locations

After P- and S-phase onset times were determined, hypocenters were located using a linearized inversion method (for details see Baisch et al., 2002). The underlying seismic velocity model was adopted from previous studies, where average velocities have been calibrated by associating the location of early seismicity with the flow exit at the wellbore (compare Baisch et al., 2006). The velocity model (listed in Table 6) is based on calibration data obtained from the stimulation of the neighbouring well Habanero#3 (Baisch & Rothert, 2010).

For the hypocenter location a minimum number of 8 phase onset times was required including at least 2 S-phase readings. Solutions were discarded whenever the formal location error (determined from projecting the data misfit into the model space, compare Baisch et al., 2002) exceeded 150 m on a 1-σ level into any spatial direction. Averaged

formal location errors on a 1-σ level are 41 m, 38 m, and 68 m into eastern, northern, and vertical direction, respectively. These error estimates do not include a potential bias resulting from inaccuracies of the assumed seismic velocity structure.

Figure 10 shows the spatial distribution of the 20,734 seismic events for which hypocenters could be determined. The resulting seismicity forms a subhorizontal cloud around the injection well with a lateral extension of 1 times 2 kilometres. The (apparent) vertical extension is in the order of several hundreds of metres and is dominated by the hypocenter location accuracy. Seismic activity is highly organized in space and time, starting close to the injection well and subsequently migrating away. These characteristics are consistent with previous observations made during hydraulic stimulations in the same reservoir.

We note that the induced seismicity near Habanero#4 is located approx. 70 m below the known fracture intersection (Figure 10, bottom) indicating that the seismic velocity model is not strictly accurate near the Habanero#4 wellbore. Furthermore, we note that the hypocenter location accuracy is decreasing for the more distant events located at the northern rim of the stimulated reservoir. Sensitivity tests performed during real-time monitoring revealed that the hypocentral depth for these events is critically depending on S-phase readings at station MW1.

A more detailed analysis of the single station impact on hypocenter locations and a re-calibration of the seismic velocity model were performed after the monitoring operation and are documented in a separate report (GDY035). The resulting velocity model is listed in Table 6.

station	Vp [m/s]	Vs [m/s]
WA01	3660 (3603)	1926 (1901)
WA02	3660 (3615)	1926 (1923)
WA03	3478 (3465)	1831 (1809)
WA04	3660 (3641)	1926 (1915)
MW01	3607 (3485)	1898 (1857)
MW02	3287 (3314)	1730 (1708)
MW03	3461 (3409)	1822 (1780)

Table 6: Station dependent seismic velocity model assumed for determining hypocenter locations. Seismic velocities resulting from re-calibration (documented in GDY035) are shown in brackets.
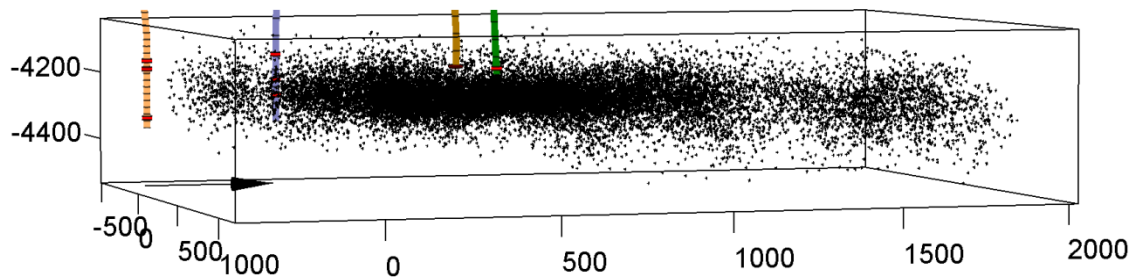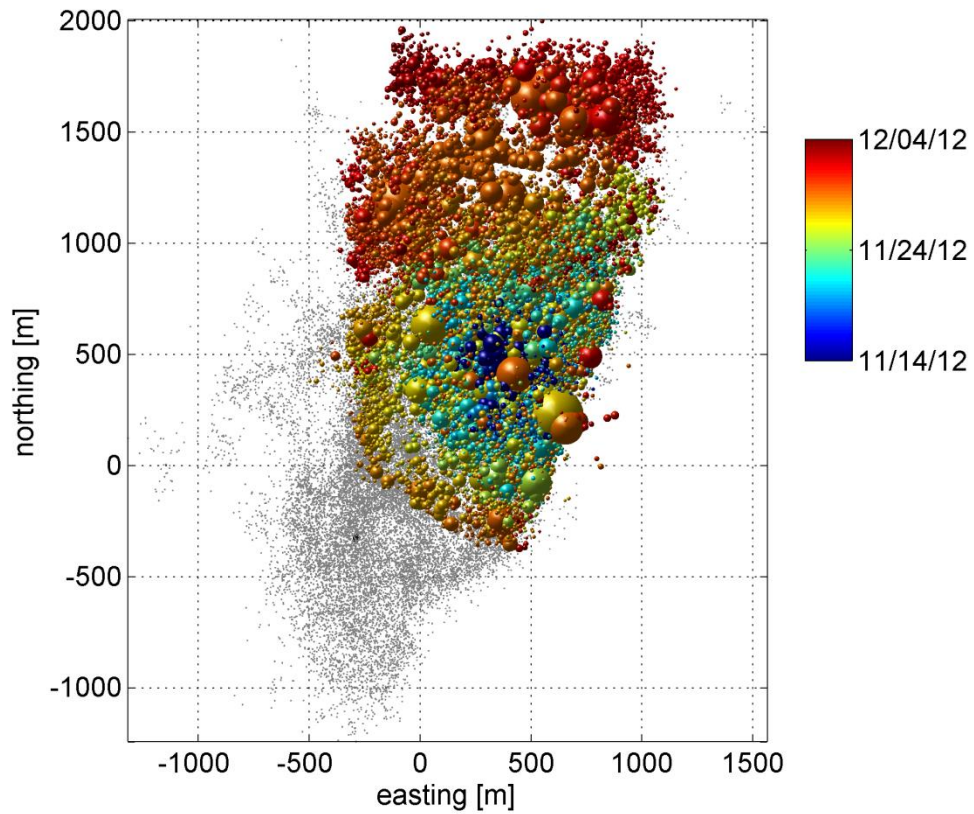
Figure 10: (top:) Hypocenter locations of the induced seismicity in map view. Each of the 20,734 seismic events is displayed by a globe scaled to the event magnitude. Color encoding denotes occurrence time according to the legend. Previous seismic activity is indicated by grey dots. (bottom:) Hypocenter locations in side-view looking from ESE. Seismic events are displayed as dots. The trajectory of the Habanero#1, #2, #3, #4 well (left to right) is displayed by colored lines. Known fracture intersections are indicated in red. Note that the induced seismicity near Habanero#4 (green trajectory) on average is located approx. 70 m below the known fracture intersection. This indicates a systematic bias of hypocentral depths introduced by the assumed velocity model.

3.2.4 Magnitude Determination

For each event detection, the local magnitude M_L was automatically determined using

Equation 1
$$M_L = log_{10}\left(\frac{\overline{PGV}}{\overline{PGV}_{cal}}\right) + M_{cal}$$

with $\overline{PGV}$ denoting the peak ground velocity determined by averaging the measured maximum signal amplitude over all recording channels. Correspondingly, $\overline{PGV}_{cal}$ denotes the network averaged peak ground velocity of a calibration event of magnitude M_{cal}. The calibration event data was taken from a previous stimulation campaign in the same reservoir (for details see Baisch et al., 2009), where several of the largest magnitude events were also recorded by Geoscience Australia. Using event magnitudes determined by Geoscience Australia, we obtain $\overline{PGV}_{cal}$=5.2 mm/s for a calibration event with magnitude M_{cal}=2.9. Note that $\overline{PGV}_{cal}$ was measured by the same local seismic monitoring stations used during the current monitoring campaign. Assuming that average hypocentral distances to the stations are the same as for the calibration event, M_L determined for the current seismicity should be consistent with the magnitude scale of Geoscience Australia. Furthermore, M_L provides a robust magnitude estimate during automatic processing even when a hypocenter location could not be determined. Therefore, the operation of the traffic light system (section 3.2.5) was based on the M_L scale.

Figure 11 shows magnitude M_L as a function of time for all detected seismic events. The maximum event magnitude is M_L=3.0.

Thirty of the strongest seismic events were also detected by the permanent station network operated by Geoscience Australia. Magnitudes determined by Geoscience Australia are significantly larger than M_L determined with the local monitoring stations (Figure 12). This is surprising since the M_L scale was calibrated against the magnitude scale of Geoscience Australia (as of 2005).

To further investigate this discrepancy we calculated the moment magnitude from displacement spectra (following the definition of Hanks & Kanamori, 1979) and the Richter magnitude (Richter, 1935). For the strongest event we obtain a moment magnitude of M_w=2.9 and a Richter magnitude of M=3.3 (Figure 13). Although the Richter magnitude is slightly larger than the local magnitude M_L=3.0 determined for this event, we note that the three different types of magnitude determined from recordings of the local station network are relatively consistent and differ significantly from the magnitudes determined by Geoscience Australia.

Furthermore, we note that the relative order of the Geoscience Australia magnitudes is not consistent with signal amplitudes measured with the local monitoring stations. This is demonstrated in Figure 14 (top) where measured peak ground velocity (PGV) is plotted

against magnitude. Two different definitions of PGV have been used: firstly, PGV is determined by the maximum ground velocity measured by any of the local stations (blue dots), and secondly PGV is determined by averaging maximum ground velocity over the station network. Independent of the definition of PGV, there appears no clear relationship between PGV and the magnitudes assigned by Geoscience Australia (Figure 14, top). In contrast, a clear relation between PGV and magnitudes is observed when using the local magnitude scale M_L (Figure 14, bottom).

The lack of internal consistency of the magnitudes assigned by Geoscience Australia may indicate that their magnitude estimates are less robust due to the large distance of their closest monitoring stations.

Alternatively, source directivity effects as well as the different recording frequency range (the local monitoring stations have comparatively large eigenfrequencies, see section 5) may account for differences of the magnitude estimates.
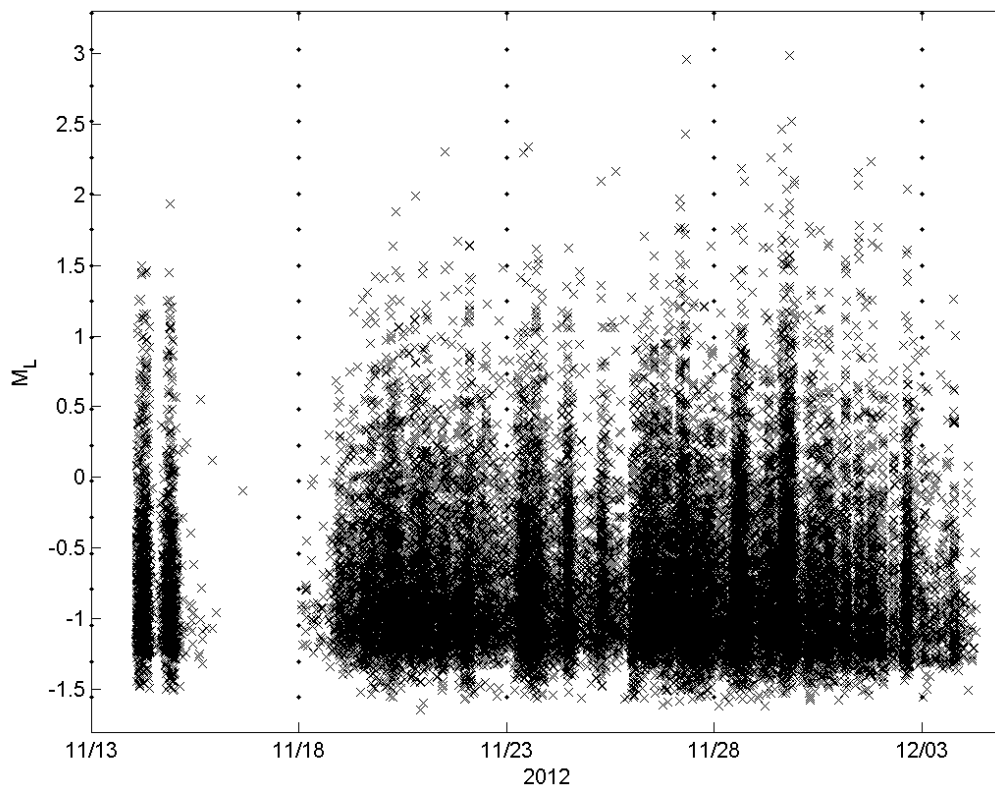
Figure 11: Magnitude M_L of all 27,445 seismic events as a function of time.
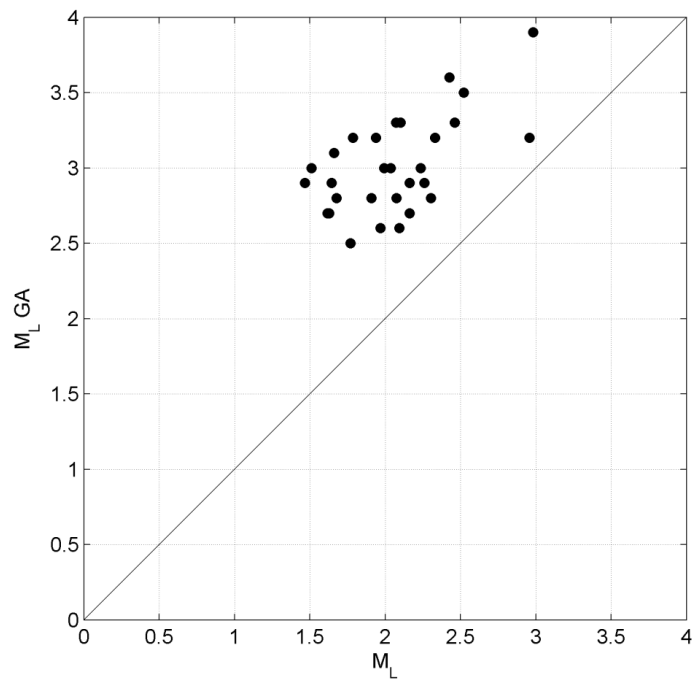
Figure 12: Comparison between the local magnitude M_L and magnitudes assigned by Geoscience Australia M_L GA (black dots) for those 30 seismic events which were recorded by Geoscience Australia. Note that the magnitudes assigned by Geoscience Australia are systematically larger than the magnitude determined with the local station network.
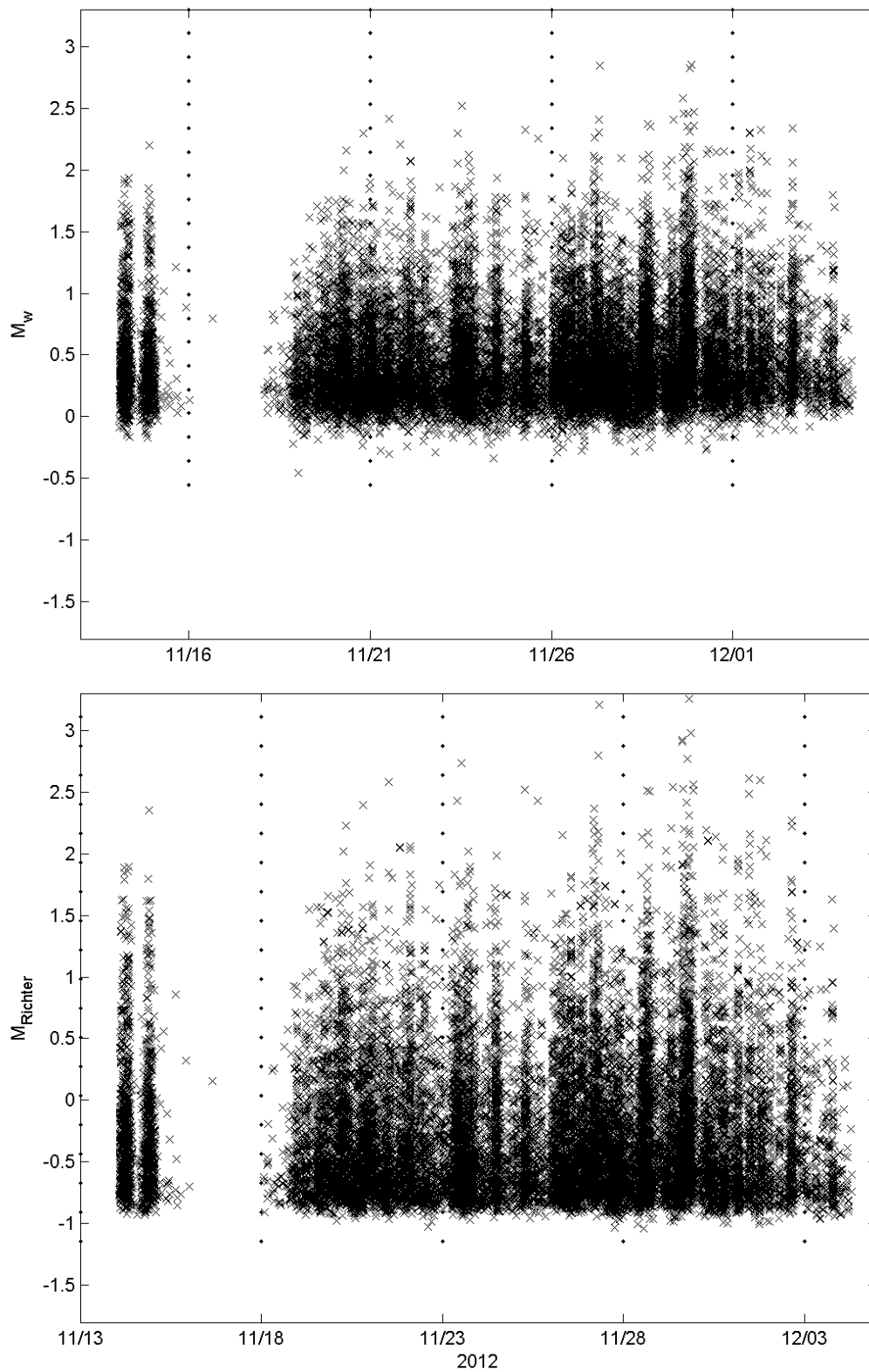
Figure 13: Moment magnitude M_w (top) and Richter magnitude (bottom) as a function of time for the 20,734 seismic events for which hypocenter locations could be determined.
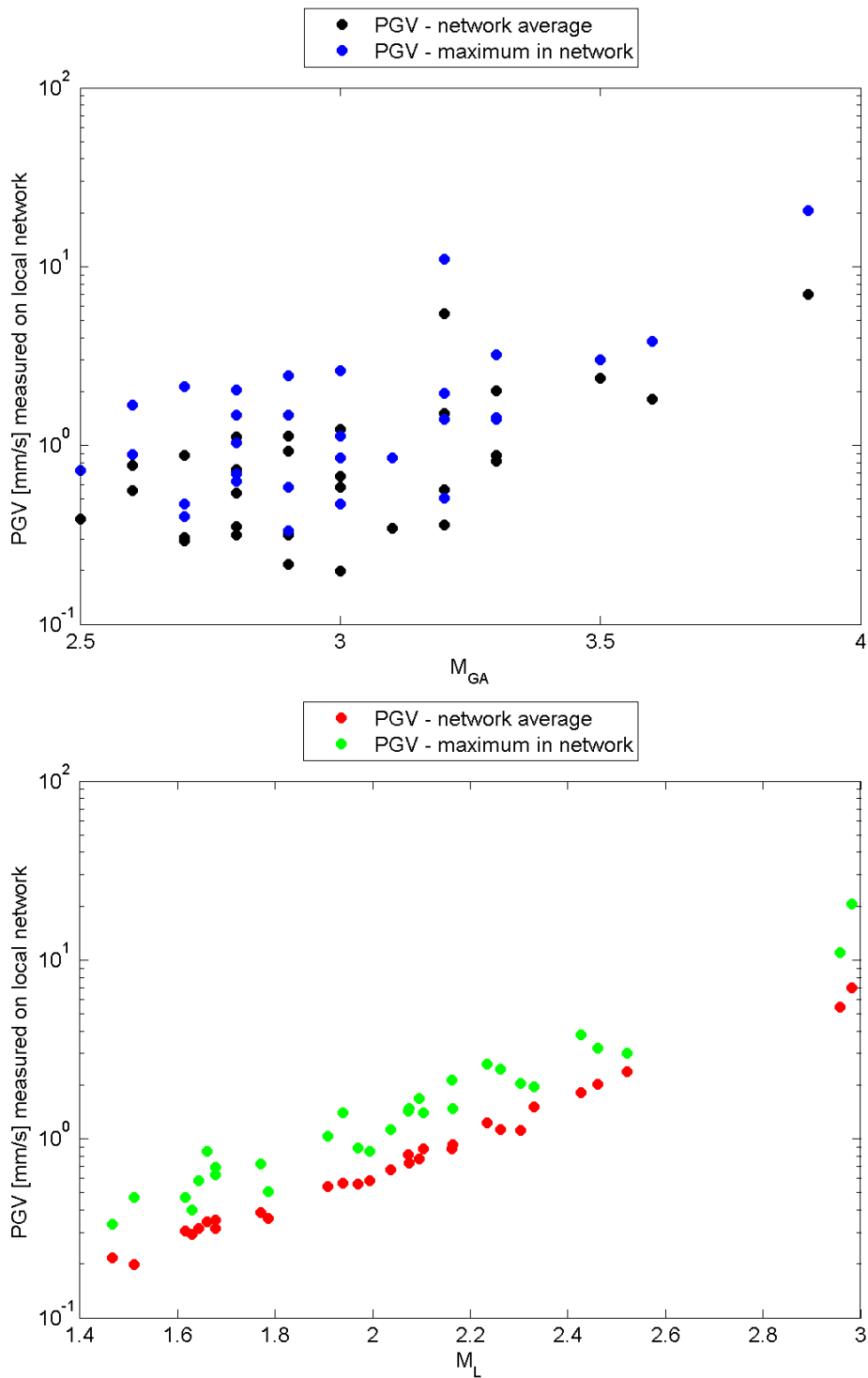
Figure 14: Peak ground velocity measured by the local stations plotted against event magnitude M_{GA} assigned by Geoscience Australia (top) and against the local magnitude M_L (bottom).

3.2.5 Traffic Light System

During real-time monitoring the QUBE traffic light system was operated to stop hydraulic operations in case the magnitude of the induced seismicity reached the pre-defined critical level of M_L=3.7 (red traffic light). Furthermore, the yellow traffic light status was defined for events with $M_L \geq 2.5$.

Whenever a potential traffic light event was detected by automatic processing, the event was assigned priority in the data base for immediate quality control. After visual inspection, traffic light events were reported immediately (i.e. all traffic light events were reported within less than 4 minutes after the event has occurred) to the operations manager and to the Geodynamics reservoir engineering team. For this, the seismic acquisition office operated a permanent radio link to the operations manager. Additionally, the operations manager could be contacted by (portable) telephone from the Q-con office in Germany.

The following (yellow) traffic light events were reported during real-time monitoring:

1. November 27th, 2012 08:03 UTC: M_L=3.0
2. November 29th, 2012 14:53 UTC: M_L=2.5
3. November 29th, 2012 19:21 UTC: M_L=3.0
4. November 29th, 2012 20:31 UTC: M_L=2.5

and the reported event parameters were

- magnitude M_L,
- occurrence time,
- hypocenter location and confidence limits,
- and traffic light status.

The first traffic light event, which occurred on November 27th, 2012, was not automatically located. Even after quality control by an experienced seismologist, S-phase onset times could not be unambiguously identified due to comparatively complex seismograms. Therefore, only the epicentre of the event, which was determined using P-phase onsets only, was reported in real-time. The hypocenter of the event could be determined only after a more sophisticated analysis was performed based on waveform polarity characteristics. The resulting hypocenter location was reported to Geodynamics Ltd. as part of the daily monitoring journals (see Section 6).

Failure of 4 or more live stations was also defined as a red traffic light event. On November 19th, 2012 (19:50 UTC) the main radio dropped out corresponding to a failure of all seismic stations. The field seismologist immediately fixed the issue by rebooting the device. He

decided not to declare the failure as a red traffic light event since the real-time data stream was re-established within approx. 3 minutes and the previous data gap was backfilled and processed after approx. 5 minutes.

4   REFERENCES

Baisch, S., Bohnhoff, M., Ceranna, L., Tu, Y., and H.-P.Harjes, 2002. Probing the crust to 9 km depth: Fluid injection experiments and induced seismicity at the KTB super-deep drilling hole, Germany. *Bull. Seism. Soc. Amer.*, **92**, 2369 – 2380.

Baisch, S., Weidler, R., Vörös, R., Wyborn, D., and L. DeGraaf, 2006. Induced seismicity during the stimulation of a geothermal HFR reservoir in the Cooper Basin (Australia). *Bull. Seism. Soc. Amer.*, 96 (6), 2242-2256.

Baisch, S., Vörös, R., Weidler, R., and D., Wyborn, 2009. Investigation of Fault Mechanisms during Geothermal Reservoir Stimulation Experiments in the Cooper Basin (Australia). *Bull. Seism. Soc. Amer.*, **99** (1), 148-158.

Baisch, S., and E. Rothert, 2010. Seismic Monitoring Report SMR-GDY049 prepared for Geodynamics Ltd., 32 pages.

Hanks, T. C. & Kanamori, H., 1979. A moment magnitude scale. Jour. Geophys. Res., 84, 2348-2350.

Richter, C. F., 1935. An instrumental earthquake magnitude scale. *Bull. Seism. Soc. Amer.*, 25 (1), 1-32.

5 STATION SPECIFICATION SHEETS

Note that for all stations except for WA03 the effective LSB of the data header (cd1.1) needs to be doubled because the specific type of ADC boards used here has a peak-to-peak range of 40 V. In the firmware configuration of the data loggers, a peak-to-peak range of 20 V is assumed.

5.1 Station WA01

station WA01	
type of station	live
location lat / lon	-27.78580679° / 140.71804801°
deployment depth	48.08 m BSL
sensor type	manufactured by CRIEPI (Central Research Institute of the Electric Power Industry of Japan)
eigenfrequency	~ 5 Hz
sensitivity	160 V/m/s
instrument polarity	flipped
data logger	Smart-24R® (Geotech Instruments, LLC)
sampling rate	500 Hz
gain	8
effective LSB – ch1	2*0.204661 μV/cnt
effective LSB – ch2	2*0.204727 μV/cnt
effective LSB – ch3	2*0.204626 μV/cnt

5.2 Station WA02

station WA02	
type of station	live
location lat / lon	-27.82190471° / 140.70514365°
deployment depth	48.75 m BSL
sensor type	manufactured by CRIEPI (Central Research Institute of the Electric Power Industry of Japan)
eigenfrequency	~ 5 Hz
sensitivity	160 V/m/s
instrument polarity	normal
data logger	Smart-24R® (Geotech Instruments, LLC)
sampling rate	500 Hz
gain	8
effective LSB – ch1	2*0.204656 μV/cnt
effective LSB – ch2	2*0.204685 μV/cnt
effective LSB – ch3	2*0.204607 μV/cnt

5.3 Station WA03

station WA03	
type of station	live
location lat / lon	-27.86011857° / 140.75167968°
deployment depth	59.33 m ASL
sensor type (before December 3rd, 2012)	Geotech S-13 short period surface seismometer (3-component)
sensor type (after December 3rd, 2012)	LE-3Dlite MkII (Lennartz electronic GmbH)
eigenfrequency	1 Hz
sensitivity (before December 3rd, 2012)	V = 623 V/m/s H1 = 616 V/m/s H2 = 614 V/m/s
sensitivity (after December 3rd, 2012)	400 V/m/s
instrument polarity	normal
data logger	Smart-24R® (Geotech Instruments, LLC)
sampling rate	500 Hz
gain	1
effective LSB – ch1	3.317024 μV/cnt
effective LSB – ch2	3.300552 μV/cnt
effective LSB – ch3	3.309472 μV/cnt

The Geotech S-13 sensor was replaced on December 3rd, 2012 by a LE-3Dlite MkII (Lennartz electronic GmbH) seismometer.

5.4 Station WA04

Note: The channel order in the cd1.1 data files is h1, v, h2.

station WA04	
type of station	live
location lat / lon	-27.78184571° / 140.78740344°
deployment depth	22.71 m BSL
sensor type	manufactured by CRIEPI (Central Research Institute of the Electric Power Industry of Japan)
eigenfrequency	~ 5 Hz
sensitivity	160 V/m/s
instrument polarity	normal
data logger	Smart-24R® (Geotech Instruments, LLC)
sampling rate	500 Hz
gain	8
effective LSB – ch1	2*0.204749 μV/cnt
effective LSB – ch2	2*0.204654 μV/cnt
effective LSB – ch3	2*0.204062 μV/cnt

5.5 Station MW01

station MW01	
type of station	live
location lat / lon	-27.79923486° / 140.75463047°
deployment depth	305.01 m BSL
sensor type	ASL Avalon Sciences Ltd. PSS-1 (SM-4-HT)
eigenfrequency	10 Hz
sensitivity	80 V/m/s
instrument polarity	normal
data logger	Smart-24R® (Geotech Instruments, LLC)
sampling rate	500 Hz
gain	8
effective LSB – ch1	2*0.204642 μV/cnt
effective LSB – ch2	2*0.204643 μV/cnt
effective LSB – ch3	2*0.204600 μV/cnt

5.6 Station MW02

station MW02	
type of station	live
location lat / lon	27.83026026° / 140.74197245°
deployment depth	56.29 m ASL
sensor type	ASL Avalon Sciences Ltd. PSS-1 (SM-4-HT)
eigenfrequency	10 Hz
sensitivity	80 V/m/s
instrument polarity	normal
data logger	Smart-24R® (Geotech Instruments, LLC)
sampling rate	500 Hz
gain	8
effective LSB – ch1	2*0.207375 μV/cnt
effective LSB – ch2	2*0.206343 μV/cnt
effective LSB – ch3	2*0.206752 μV/cnt

5.7 Station MW03

station MW03	
type of station	live
location lat / lon	-27,82885987° / 140,76823367°
deployment depth	172.30 m BSL
sensor type	ASL Avalon Sciences Ltd. PSS-1 (SM-4-HT)
eigenfrequency	10 Hz
sensitivity	80 V/m/s
instrument polarity	normal
data logger	Smart-24R® (Geotech Instruments, LLC)
sampling rate	500 Hz
gain	8
effective LSB – ch1	2*0.207377 μV/cnt
effective LSB – ch2	2*0.206567 μV/cnt
effective LSB – ch3	2*0.206595 μV/cnt

5.8 Station MS01

station MS01	
type of station	offline
location lat / lon	-27.789361° / 140.675639°
deployment depth	57.7 m BSL
sensor type	Geosym GmbH passive seismic sonde
eigenfrequency	4.5 Hz
sensitivity	96 V/m/s
instrument polarity	normal
data logger	Smart-24R® (Geotech Instruments, LLC)
sampling rate	500 Hz
gain	8
effective LSB – ch1	2*0.2044945 μV/cnt
effective LSB – ch2	2*0.2043450 μV/cnt
effective LSB – ch3	2*0.2043105 μV/cnt

5.9 Station MS02

station MS02	
type of station	offline
location lat / lon	-27.796056° / 140.640222°
deployment depth	76.5 m BSL
sensor type	Geosym GmbH passive seismic sonde
eigenfrequency	4.5 Hz
sensitivity	96 V/m/s
instrument polarity	normal
data logger	Smart-24R® (Geotech Instruments, LLC)
sampling rate	500 Hz
gain	8
effective LSB – ch1	2*0.2045275 μV/cnt
effective LSB – ch2	2*0.2047350 μV/cnt
effective LSB – ch3	2*0.2040195 μV/cnt

5.10 Station MS03

station MS03	
type of station	offline
location lat / lon	-27.820000° / 140.670000°
deployment depth	35.5 m BSL
sensor type	Geosym GmbH passive seismic sonde
eigenfrequency	4.5 Hz
sensitivity	96 V/m/s
instrument polarity	normal
data logger	Smart-24R® (Geotech Instruments, LLC)
sampling rate	500 Hz
gain	8
effective LSB – ch1	2*0.2044840 μV/cnt
effective LSB – ch2	2*0.2043820 μV/cnt
effective LSB – ch3	2*0.2043275 μV/cnt

5.11 Station MS04

station MS04	
type of station	offline
location lat / lon	-27.760556° / 140.648889°
deployment depth	59.5 m BSL
sensor type	Geosym GmbH passive seismic sonde
eigenfrequency	4.5 Hz
sensitivity	96 V/m/s
instrument polarity	normal
data logger	Smart-24R® (Geotech Instruments, LLC)
sampling rate	500 Hz
gain	8
effective LSB – ch1	2*0.2045115 μV/cnt
effective LSB – ch2	2*0.2043345 μV/cnt
effective LSB – ch3	2*0.2041980 μV/cnt

5.12 Station MS05

station MS05	
type of station	offline
location lat / lon	-27.831611° / 140.631667°
deployment depth	82.5 m BSL
sensor type	Geosym GmbH passive seismic sonde
eigenfrequency	4.5 Hz
sensitivity	96 V/m/s
instrument polarity	normal
data logger	Smart-24R® (Geotech Instruments, LLC)
sampling rate	500 Hz
gain	8
effective LSB – ch1	2*0.2043690 μV/cnt
effective LSB – ch2	2*0.2044515 μV/cnt
effective LSB – ch3	2*0.2041195 μV/cnt

5.13 Station MS06 (Innamincka Pub)

station MS06	
type of station	offline
location lat / lon	-27.746330° / 140.737876°
deployment depth	57.5 m ASL
sensor type	LE-3Dlite MkII (Lennartz electronic GmbH)
eigenfrequency	1.00 Hz
sensitivity	400 V/m/s
instrument polarity	normal
data logger	Smart-24R® (Geotech Instruments, LLC)
sampling rate	500 Hz
gain	8
effective LSB – ch1	2*0.2074885 µV/cnt
effective LSB – ch2	2*0.2073440 µV/cnt
effective LSB – ch3	2*0.2061985 µV/cnt

The station was decommissioned on December 3rd, 2012.

5.14 Station MS07

station MS07	
type of station	offline
location lat / lon	-27.81267° / 140.57489°
deployment depth	82.0 m BSL
sensor type	Geosym GmbH passive seismic sonde
eigenfrequency	4.5 Hz
sensitivity	96 V/m/s
instrument polarity	flipped
data logger	Smart-24R® (Geotech Instruments, LLC)
sampling rate	500 Hz
gain	8
effective LSB – ch1	2*0.2053025 μV/cnt
effective LSB – ch2	2*0.2049910 μV/cnt
effective LSB – ch3	2*0.2051115 μV/cnt

5.15 Station MS08

station MS08	
type of station	offline
location lat / lon	-27.83780° / 140.58702°
deployment depth	72.0 m BSL
sensor type	Geosym GmbH passive seismic sonde
eigenfrequency	4.5 Hz
sensitivity	96 V/m/s
instrument polarity	normal
data logger	Smart-24R® (Geotech Instruments, LLC)
sampling rate	500 Hz
gain	8
effective LSB – ch1	2*0.2046545 μV/cnt
effective LSB – ch2	2*0.2047570 μV/cnt
effective LSB – ch3	2*0.2045885 μV/cnt

5.16 Station MS09

station MS09	
type of station	offline
location lat / lon	-27.83096° / 140.55295°
deployment depth	79.5 m BSL
sensor type	Geosym GmbH passive seismic sonde
eigenfrequency	4.5 Hz
sensitivity	96 V/m/s
instrument polarity	normal
data logger	Smart-24R® (Geotech Instruments, LLC)
sampling rate	500 Hz
gain	8
effective LSB – ch1	2*0.2046525 μV/cnt
effective LSB – ch2	2*0.2047225 μV/cnt
effective LSB – ch3	2*0.2046285 μV/cnt

5.17 Station SS01

station SS01	
type of station	offline
location lat / lon	-27.862694° / 140.682144°
deployment depth	48.5 m ASL
sensor type	LE-3Dlite MkII (Lennartz electronic GmbH)
eigenfrequency	1.00 Hz
sensitivity	400 V/m/s
instrument polarity	normal
data logger	Smart-24R® (Geotech Instruments, LLC)
sampling rate	500 Hz
gain	1
effective LSB – ch1	2*1.6354680 μV/cnt
effective LSB – ch2	2*1.6357041 μV/cnt
effective LSB – ch3	2*1.6362120 μV/cnt

5.18 Station SS02

station SS02	
type of station	offline
location lat / lon	-27.871545° / 140.837341°
deployment depth	61.5 m ASL
sensor type	LE-3Dlite MkII (Lennartz electronic GmbH)
eigenfrequency	1.00 Hz
sensitivity	400 V/m/s
instrument polarity	normal
data logger	Smart-24R® (Geotech Instruments, LLC)
sampling rate	500 Hz
gain	1
effective LSB – ch1	2*1.6365041 μV/cnt
effective LSB – ch2	2*1.6392040 μV/cnt
effective LSB – ch3	2*1.6359720 μV/cnt

5.19 Station SS03

station SS03	
type of station	offline
location lat / lon	-27.795458° / 140.815580°
deployment depth	71.5 m ASL
sensor type	LE-3Dlite MkII (Lennartz electronic GmbH)
eigenfrequency	1.00 Hz
sensitivity	400 V/m/s
instrument polarity	normal
data logger	Smart-24R® (Geotech Instruments, LLC)
sampling rate	500 Hz
gain	1
effective LSB – ch1	2*1.6385561 μV/cnt
effective LSB – ch2	2*1.6364321 μV/cnt
effective LSB – ch3	2*1.6359801 μV/cnt

5.20 Station SS04

station SS04	
type of station	offline
location lat / lon	-27.741249° / 140.842801°
deployment depth	68.5 m ASL
sensor type	LE-3Dlite MkII (Lennartz electronic GmbH)
eigenfrequency	1.00 Hz
sensitivity	400 V/m/s
instrument polarity	normal
data logger	Smart-24R® (Geotech Instruments, LLC)
sampling rate	500 Hz
gain	1
effective LSB – ch1	2*1.6367040 μV/cnt
effective LSB – ch2	2*1.6431001 μV/cnt
effective LSB – ch3	2*1.6345881 μV/cnt

5.21 Station SS05

station SS05	
type of station	offline
location lat / lon	-27.715496° / 140.760285°
deployment depth	82.5 m ASL
sensor type	LE-3Dlite MkII (Lennartz electronic GmbH)
eigenfrequency	1.00 Hz
sensitivity	400 V/m/s
instrument polarity	normal
data logger	Smart-24R® (Geotech Instruments, LLC)
sampling rate	500 Hz
gain	1
effective LSB – ch1	2*1.6376081 µV/cnt
effective LSB – ch2	2*1.6390561 µV/cnt
effective LSB – ch3	2*1.6356920 µV/cnt

5.22 Station SS06

station SS06	
type of station	offline
location lat / lon	-27.684270° / 140.684396°
deployment depth	52.5 m ASL
sensor type	LE-3Dlite MkII (Lennartz electronic GmbH)
eigenfrequency	1.00 Hz
sensitivity	400 V/m/s
instrument polarity	normal
data logger	Smart-24R® (Geotech Instruments, LLC)
sampling rate	500 Hz
gain	1
effective LSB – ch1	2*1.6384880 μV/cnt
effective LSB – ch2	2*1.6373481 μV/cnt
effective LSB – ch3	2*1.6368760 μV/cnt

5.23 Station SS07

station SS07	
type of station	offline
location lat / lon	-27.684582° / 140.605396°
deployment depth	49.5 m ASL
sensor type	LE-3Dlite MkII (Lennartz electronic GmbH)
eigenfrequency	1.00 Hz
sensitivity	400 V/m/s
instrument polarity	normal
data logger	Smart-24R® (Geotech Instruments, LLC)
sampling rate	500 Hz
gain	1
effective LSB – ch1	2*1.6367001 μV/cnt
effective LSB – ch2	2*1.6363881 μV/cnt
effective LSB – ch3	2*1.6369081 μV/cnt

5.24 Station SS08

station SS07	
type of station	offline
location lat / lon	-27.721203° / 140.588354°
deployment depth	49.5 m ASL
sensor type	LE-3Dlite MkII (Lennartz electronic GmbH)
eigenfrequency	1.00 Hz
sensitivity	400 V/m/s
instrument polarity	normal
data logger	Smart-24R® (Geotech Instruments, LLC)
sampling rate	500 Hz
gain	1
effective LSB – ch1	2*1.6382720 μV/cnt
effective LSB – ch2	2*1.6384240 μV/cnt
effective LSB – ch3	2*1.6382280 μV/cnt

6 APPENDIX: LIST OF DAILY MONITORING REPORTS

Report name	Reporting time UTC		Reporting time ACST (local)		Report date (UTC)
121113_SMJ_GDY0136	12-11-2012 13:30	13-11-2012 13:30	13-11-2012 00:00	14-11-2012 00:00	13-11-2012
121114_SMJ_GDY0137	13-11-2012 13:30	14-11-2012 13:30	14-11-2012 00:00	15-11-2012 00:00	14-11-2012
121115_SMJ_GDY0138	14-11-2012 13:30	15-11-2012 13:30	15-11-2012 00:00	16-11-2012 00:00	15-11-2012
121116_SMJ_GDY0139	15-11-2012 13:30	16-11-2012 13:30	16-11-2012 00:00	17-11-2012 00:00	16-11-2012
121117_SMJ_GDY0140	16-11-2012 13:30	17-11-2012 13:30	17-11-2012 00:00	18-11-2012 00:00	17-11-2012
121118_SMJ_GDY0141	17-11-2012 13:30	18-11-2012 13:30	18-11-2012 00:00	19-11-2012 00:00	18-11-2012
121119_SMJ_GDY0142	18-11-2012 13:30	19-11-2012 13:30	19-11-2012 00:00	20-11-2012 00:00	19-10-2012
121120_SMJ_GDY0143	19-11-2012 13:30	20-11-2012 13:30	20-11-2012 00:00	21-11-2012 00:00	20-11-2012
121121_SMJ_GDY0144	20-11-2012 13:30	21-11-2012 13:30	21-11-2012 00:00	22-11-2012 00:00	21-11-2012
121122_SMJ_GDY0145	21-11-2012 13:30	22-11-2012 13:30	22-11-2012 00:00	23-11-2012 00:00	22-11-2012
121123_SMJ_GDY0146	22-11-2012 13:30	23-11-2012 13:30	23-11-2012 00:00	24-11-2012 00:00	23-11-2012
121124_SMJ_GDY0147	23-11-2012 13:30	24-11-2012 13:30	24-11-2012 00:00	25-11-2012 00:00	24-11-2012
121125_SMJ_GDY0148	24-11-2012 13:30	25-11-2012 13:30	25-11-2012 00:00	26-11-2012 00:00	25-11-2012

Report name	Reporting time UTC		Reporting time ACST (local)		Report date (UTC)
121126_SMJ_GDY0149	25-11-2012 13:30	26-11-2012 13:30	26-11-2012 00:00	27-11-2012 00:00	26-11-2012
121127_SMJ_GDY0150	26-11-2012 13:30	27-11-2012 13:30	27-11-2012 00:00	28-11-2012 00:00	27-11-2012
121128_SMJ_GDY0151	27-11-2012 13:30	28-11-2012 13:30	28-11-2012 00:00	29-11-2012 00:00	28-11-2012
121129_SMJ_GDY0152	28-11-2012 13:30	29-11-2012 13:30	29-11-2012 00:00	30-11-2012 00:00	29-11-2012
121201_SMJ_GDY0153	29-11-2012 13:30	30-11-2012 13:30	30-11-2012 00:00	01-12-2012 00:00	30-11-2012